

# 1 Direct entanglement detection of quantum systems using machine learning

2 Yulei Huang,<sup>1,2,3</sup> Liangyu Che,<sup>1,2,3</sup> Chao Wei,<sup>1,2,3</sup> Feng Xu,<sup>1,2,3</sup>  
3 Xinfang Nie,<sup>1,2,3</sup> Jun Li,<sup>1,2,3,\*</sup> Dawei Lu,<sup>1,2,3,†</sup> and Tao Xin<sup>1,2,3,‡</sup>

4 <sup>1</sup>*Shenzhen Institute for Quantum Science and Engineering and Department of Physics,*  
5 *Southern University of Science and Technology, Shenzhen 518055, China*

6 <sup>2</sup>*Guangdong Provincial Key Laboratory of Quantum Science and Engineering,*  
7 *Southern University of Science and Technology, Shenzhen 518055, China*

8 <sup>3</sup>*Shenzhen Key Laboratory of Quantum Science and Engineering,*  
9 *Southern University of Science and Technology, Shenzhen, 518055, China*

10 Entanglement is a key property in the development of quantum technologies and in the study of quantum  
11 many-body simulations. However, entanglement measurement typically requires quantum full-state tomogra-  
12 phy (FST). Here we present a neural network-assisted protocol for measuring entanglement in equilibrium and  
13 non-equilibrium states of local Hamiltonians. According to numerical simulations, comprehensive entangle-  
14 ment quantities up to 20 qubits, such as Rényi entropy, can be predicted from single-qubit and two-qubit Pauli  
15 measurements. It is also exciting that our neural network is able to learn the future entanglement dynamics  
16 using only single-qubit traces from the previous time. In addition, we perform experiments using a nuclear spin  
17 quantum processor and train an adoptive neural network to study entanglement in the ground and dynamical  
18 states of a one-dimensional spin chain. A jump across can be observed by measuring the static entanglement in  
19 the ground state as a function of the system Hamiltonian parameter, which is similar to how quantum phase transi-  
20 tions (QPT) behave in the thermodynamic limit. And the entanglement dynamics beyond measurement time  
21 is accurately estimated in dynamical states. These precise results validate our neural network. Our work will  
22 have a wide range of applications in quantum many-body systems, from quantum phase transitions to intriguing  
23 non-equilibrium phenomena such as quantum thermalization.

## 24 INTRODUCTION

25 Entanglement plays a crucial role in the development of quantum technologies [1]. It is an essential resource for simulating  
26 many-body physics [2, 3], investigating quantum advantages in quantum computation, and ensuring the security of quantum  
27 communication [4, 5]. Unfortunately, entanglement measures are not physical observables, making detection and quantification  
28 extremely challenging [6].

29 In the Noisy Intermediate-Scale Quantum (NISQ) era, new demands for quantum entanglement detection are being put forth.  
30 *Demand 1.* Quantifying entanglement effectively. Although a large number of entanglement witnesses have been constructed [7–  
31 9], some of which only require partial system information [10], they only provide a yes or no answer as to whether entanglement  
32 exists or not. Accurate quantification of entanglement, such as logarithmic negativity [11] and the PT moments [12, 13], typically  
33 requires quantum FST since there are no observables for them. However, due to the exponential increase of the number of  
34 measurements with system size, performing FST to measure entanglement will no longer be practical for NISQ devices. In recent  
35 years, a large number of methods have been proposed to boost the efficiency of FST [14–19], including compressed sensing [16],  
36 FST via local measurements [17, 18], and neural-network FST [15], but these methods may not be effective for entanglement  
37 measurement since two close states may have significantly different values of entanglement [20]. Therefore, it is increasingly  
38 essential to develop effective entanglement measurement techniques. There have been extensive studies aimed at meeting this  
39 need [21–24]. The authors use random measurements to measure the second-order Rényi entropy of subsystems [24]. *Demand*  
40 2. Detecting entanglement dynamics beyond the measurement time. Non-equilibrium quantum simulations [25–27], such as  
41 quantum thermalization, typically require long-time dynamics, but current NISQ devices still have limited coherence times.  
42 This implies that measuring long-time entanglement will be difficult. Several studies have used neural networks to investigate  
43 the long-time dynamics of local observables beyond the measurement time [28]. But it remains an open question whether it  
44 is possible to predict long-time entanglement at an unseen future time based on local measurement data in an observable time  
45 window.

46 In this work, we propose a machine learning-assisted detection protocol to determine entanglement from local measurements  
47 and validate it by quantifying the entanglement of the ground and dynamical states of the local Hamiltonian. For dynamical  
48 states, the entanglement dynamics beyond the measurement time are also accurately predicted from the single-qubit time traces  
49 only in the previous time window. Moreover, we implement an experiment to demonstrate the feasibility of our approach. We

\* [lij3@sustech.edu.cn](mailto:lij3@sustech.edu.cn)

† [ludw@sustech.edu.cn](mailto:ludw@sustech.edu.cn)

‡ [xint@sustech.edu.cn](mailto:xint@sustech.edu.cn)

50 employ it to measure static entanglement in ground states and entanglement dynamics in dynamical states of a one-dimensional  
 51 spin chain on the nuclear magnetic resonance (NMR) platform, and two-local measurements provide accurate predictions of  
 52 static entanglement as a function of system parameters. For the dynamical case, the entanglement dynamics beyond the mea-  
 53 surement time are accurately estimated from the single-qubit time traces using our machine learning approach. Our approach  
 54 offers a wide variety of applications in the study of quantum many-body entanglement.

55

## RESULTS

56

### The protocol for entanglement detection

57 The characterization and measurement of quantum entanglement is a crucial task in quantum simulation [2, 3], which typically  
 58 prepares the ground state  $\mathcal{H}|\psi_g\rangle = E_g|\psi_g\rangle$  or realizes the dynamical state  $|\psi(t)\rangle = \exp(-i\mathcal{H}t)|\psi_0\rangle$  of a given local Hamiltonian  
 59  $\mathcal{H} = \sum_{i=1}^m c_i B_i$  with Pauli basis  $B_i$ . Their entanglement can be characterized by measuring the entanglement entropy and PT  
 60 moment. The entanglement entropy provides information about the entanglement contained in the system. It is calculated  
 61 using the equation  $S^{(n)} = \frac{1}{1-n} \log(\text{tr} \rho_A^n)$ .  $\rho_A$  is the reduced density matrix of the total system  $\rho_{AB}$ . In particular,  $S^{(2)}$  is the  
 62 second-order Rényi entropy, which has been used to study entanglement growth and thermalization. The PT moment is defined  
 63 as  $\mathcal{P}_n = \text{Tr}[(\rho_{AB}^{T_A})^n]$ .  $\rho_{AB}^{T_A}$  is a partial transpose with respect to subsystem A.  $\mathcal{P}_1 = 1$ ,  $\mathcal{P}_2 = \text{Tr}[\rho_{AB}^2]$ , and  $\mathcal{P}_3$  is the lowest  
 64 PT moment that provides information about the entanglement. The first three PT moments have been used to test the bipartite  
 65 entanglement [29]. Quantum coherence in many-body simulation embodies the essence of entanglement in the following form  
 66 of  $\mathcal{C} = S(\rho_{\text{diag}}) - S(\rho)$  [30, 31].  $\rho_{\text{diag}}$  is the diagonal matrix obtained by removing all off-diagonal elements from  $\rho$ . The above  
 67 set of entanglement quantities  $\mathcal{E} \equiv \{S^{(n)}, \mathcal{P}_n, \mathcal{C}\}$  commonly requires FST or multi-copy measurements.

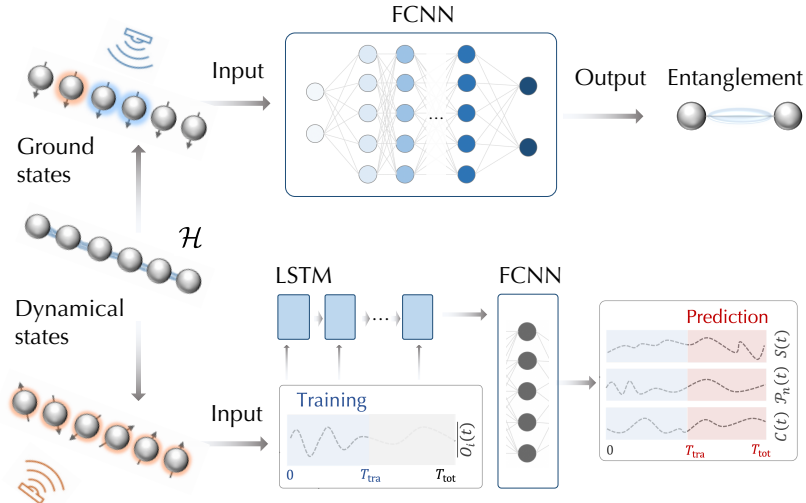


Figure 1. Schematic workflow of our neural network for learning entanglement  $\mathcal{E} \equiv \{S^{(n)}, \mathcal{P}_n, \mathcal{C}\}$  from local Pauli measurements. (a) For the ground states  $|\psi_g\rangle$ , local Pauli operators are measured and they are directly used to learn  $\mathcal{E}$  via FCNN. (b) For the dynamical states  $|\psi(t)\rangle$ , we only measure and input the expectation values of single-qubit Pauli operators in the range  $[0, T_{\text{tra}}]$ . It can predict not only the dynamics of  $\mathcal{E}$  during the training window, but also the long-time dynamics of  $\mathcal{E}$  at the unseen time  $[T_{\text{tra}}, T_{\text{tot}}]$ .

68 To avoid these issues, we use machine learning to directly predict  $\mathcal{E}$  from local Pauli measurements  $\mathcal{O}$  on the ground state  
 69  $|\psi_g\rangle$  or dynamical state  $|\psi(t)\rangle$  of the local Hamiltonian  $\mathcal{H}$ . Figure 1 presents the principle of our neural network. The nonlinear  
 70 relationship between  $\mathcal{O}$  and  $\mathcal{E}$  can be approximated by a multi-layer neural network with a finite number of neurons. This method  
 71 train a neural network with a large set of known inputs  $\mathcal{O}$  and outputs  $\mathcal{E}$ . Once the models are trained to convergence, they can  
 72 be used to experimentally predict the unknown  $\mathcal{E}$  from the measured  $\mathcal{O}$ , without quantum FST. For the ground state, the input  
 73  $\mathcal{O} = \{\langle \psi_g | B_i | \psi_g \rangle, 1 \leq i \leq m\}$  is the set of the expectation values of local Pauli operators  $B_i$  on the ground state  $|\psi_g\rangle$  and the  
 74 output is static entanglement  $\mathcal{E}$  of  $|\psi_g\rangle$ . Here, a fully-connected neural network (FCNN) is employed to map the relationship  
 75 between input  $\mathcal{O}$  and output  $\mathcal{E}$ . For the dynamical state, the input  $\mathcal{O} = \{\langle \psi_{s\tau} | \sigma_{x,y,z}^{(i)} | \psi_{s\tau} \rangle, 1 \leq s \leq S, 1 \leq i \leq N\}$  is the set  
 76 of the expectation values of single-qubit Pauli operators of each qubit at each moment  $s\tau$ .  $S$  is the number of sampling points,  
 77 and  $\tau = T_{\text{tra}}/S$  is the sampling interval. The measured data at the moment  $s\tau$  is fed into the  $s$ -th long short-term memory  
 78 (LSTM) cell before using FCNN to decode the data. The dynamical entanglement  $\mathcal{E}(t)$  is the output result. More intriguingly,  
 79 once trained, the trained model is able to predict the long-time entanglement  $\mathcal{E}(t)$  in an unseen time window  $[T_{\text{tra}}, T_{\text{tot}}]$  based

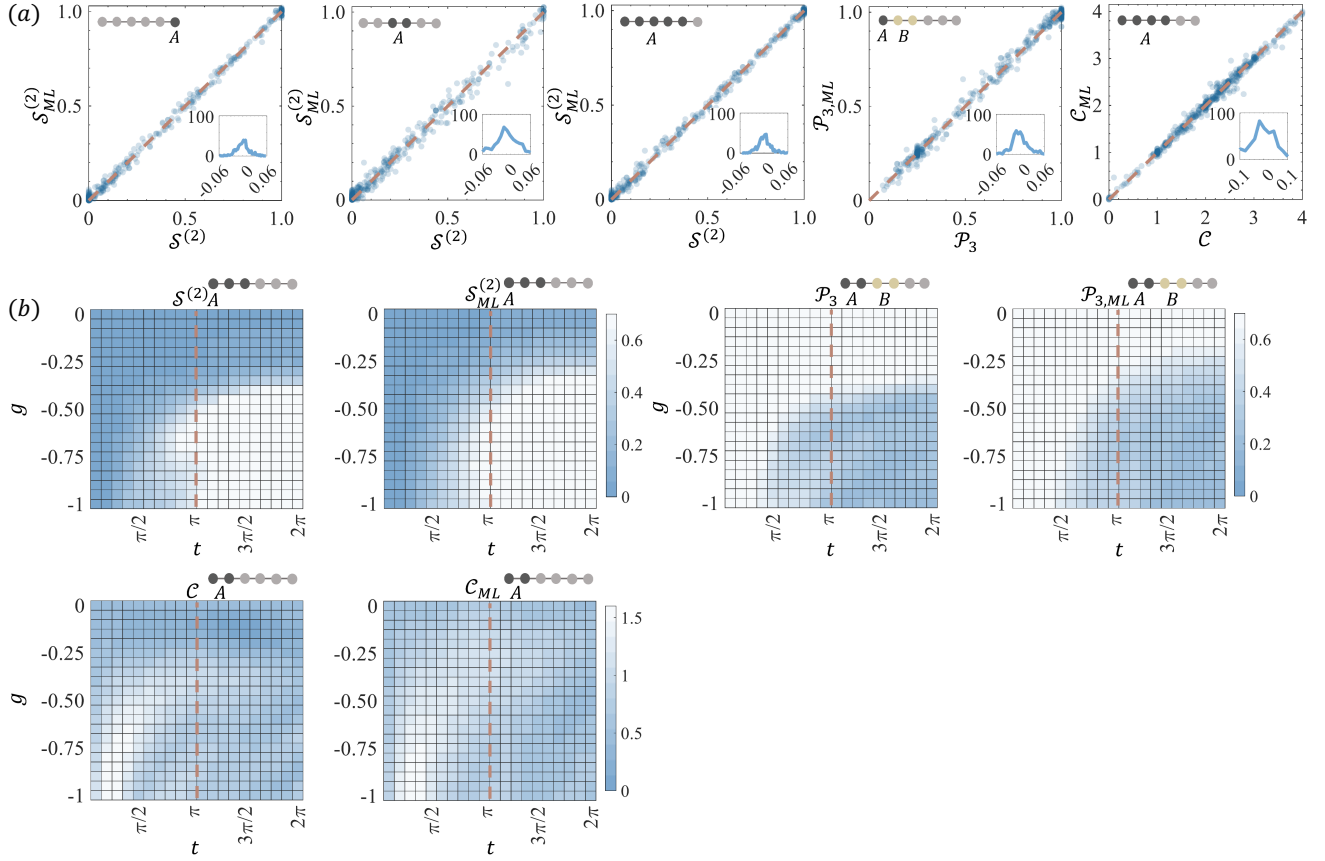


Figure 2. The entanglement estimated by machine learning. (a) The correlation figures between the predicted entanglement  $\mathcal{E}_{ML}$  from 2-local measurements and the theoretical  $\mathcal{E}$ . The inset figures are the distributions of the difference  $\mathcal{E}_{ML} - \mathcal{E}$ . (b) Prediction of entanglement dynamics  $\mathcal{E}_{ML}(t)$  from single-qubit time traces. In each pair of comparisons, the right column is the prediction result obtained by our machine learning method and the left column is the theoretical values. The input layer contains only the measured single-qubit time traces in  $[0, \pi]$ . The trained model allows us to predict  $\mathcal{E}_{ML}(t)$  at the unseen time  $[\pi, 2\pi]$ . The measured subsystems are represented by the gray rounded schematic.

on the measurement  $\mathcal{O}(t)$  in  $[0, T_{\text{tra}}]$ . This means that our neural network is able to measure the entanglement dynamics beyond the measurement time. We train the neural network using adaptive moment estimation, a well-known optimizer in machine learning. More details about our neural network can be found in [32].

83

### Numerical results

To demonstrate the feasibility of our neural network, we numerically test the following Hamiltonian models. *Model 1*. We consider a 6-qubit 2-local Hamiltonian  $\mathcal{H} = \sum_{i=1}^6 \boldsymbol{\omega}^i \cdot \boldsymbol{\sigma}^i + \sum_{j=1}^5 \boldsymbol{\sigma}^j \cdot \mathbf{J}^j \cdot \boldsymbol{\sigma}^{j+1}$  and train a neural network to predict the static  $\mathcal{E}$  of the ground states.  $\boldsymbol{\sigma}^i = (\sigma_x^i, \sigma_y^i, \sigma_z^i)$  is the vector of Pauli matrices.  $\boldsymbol{\omega}^i = (\omega_x^i, \omega_y^i, \omega_z^i)$  and  $\mathbf{J}^j = (\mathbf{J}_{xx}^j, \dots, \mathbf{J}_{zz}^j)$  represent the external magnetic field strength and the coupling tensor, respectively. During training, we generate a large number of ground states  $|\psi_g\rangle$  by randomly choosing  $\boldsymbol{\omega}, \mathbf{J} \in [-1, 1]$ , and using  $\mathcal{O}$  and  $\mathcal{E}$  of the ground states as input and output, respectively.  $\mathcal{O}$  is the set of the expectation values of the one and two-body Pauli measurements of the state, which can be easily obtained. The predicted  $\mathcal{E}$  includes the entanglement information of the subsystems. We generate 100,000 pairs of such  $(\mathcal{O}, \mathcal{E})$  for training the neural network and then randomly select 500 for testing the performance. In Fig. 2(a), we compare the estimation of  $S^{(2)}$ ,  $P_3$ , and  $C$  by our neural network with the traditional FST. *Model 2*. We train a neural network capable of predicting the entanglement dynamics of the non-equilibrium states. The system starts from  $|\psi_0\rangle = R_z(\pi/8)R_y(\pi/8)|0\rangle^{\otimes 6}$  and evolves into  $|\psi_t\rangle = \exp(-i\mathcal{H}_d t)|\psi_0\rangle$  under the Hamiltonian  $\mathcal{H}_d$ .  $\mathcal{H}_d$  is defined as  $\mathcal{H}_d = J \sum_{i=1}^5 \sigma_z^i \sigma_z^{i+1} + g \sum_{j=1}^6 \sigma_x^j$ , where  $J$  and  $g$  are adjustable parameters.  $\mathcal{H}_d$  is one of the models used in the study of entanglement dynamics [33]. We generate various  $\mathcal{H}_d$  by randomly selecting  $J$  and  $g$  between  $-1$  to  $1$ , allowing the initial state to evolve in various ways to a large number of  $|\psi_t\rangle$ . The neural network is trained by taking  $(\mathcal{O}, \mathcal{E})$  of each state at a time as input and output. This model differs from the previous one

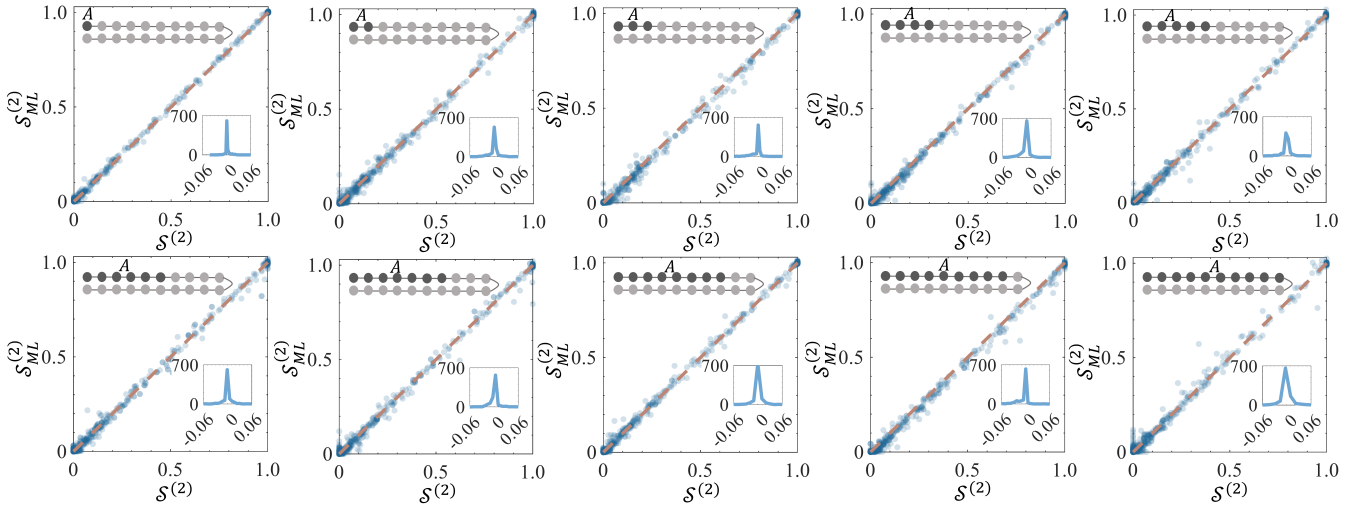


Figure 3. The correlation figures between the predicted  $S_{ML}^{(2)}$  from 2-local measurements and the theoretical  $\mathcal{S}$  for the test 20-spin systems. The measured subsystems are represented by the gray rounded schematic. We randomly select 1000 for testing the performance after our neural networks are trained. The inset figures are the distributions of the difference  $S_{ML}^{(2)} - \mathcal{S}$ .

in that we use only single-qubit Pauli measurements. The predicted  $\mathcal{E}$  includes the entanglement dynamics of the subsystems. Here, we still use 100,000 data for training the neural network, and we only feed  $\mathcal{O}$  in the previous time  $[0, \pi]$  as the input during training. The output is the entanglement dynamics  $\mathcal{E}(t)$  in a longer time range  $[0, 2\pi]$ . We set  $J = -0.5$  and divide  $g$  from  $-1$  to  $0$  into 20 parts to generate 20 pieces of data to test our neural network. Figure 2(b) depicts the predicted  $S^{(2)}(t)$ ,  $\mathcal{P}_3(t)$ , and  $\mathcal{C}(t)$  for the time interval  $[0, 2\pi]$ . It is shown that  $\mathcal{E}(t)$  can be accurately predicted from the single-qubit time traces [33].

*For 20-spin systems*-. To test the feasibility of our machine learning method in large systems, we employ a tensor network-based simulation approach to train our machine learning model for systems with up to 20 spins. Similarly, we consider a 20-qubit 2-local Hamiltonian model

$$\mathcal{H} = \sum_{i=1}^{20} \boldsymbol{\omega}^i \cdot \boldsymbol{\sigma}^i + \sum_{j=1}^{19} \boldsymbol{\sigma}^j \cdot \mathbf{J}^j \cdot \boldsymbol{\sigma}^{j+1}. \quad (1)$$

We use the tensor network to randomly generate the ground states of 20-spins Hamiltonians for training the neural network. The input data set contains the Pauli measurement information of the single-qubit and the nearest two-qubits, and the output data set contains the Rényi entropy of the sequential subsystems ( $A = 1, 12, 123, 1234, etc$ ) until the front 10-qubit subsystem. After successfully training the neural network for 20-spin systems, we randomly select 1000 test dataset to test the performance of trained neural networks. In Fig. 3, we compared the estimation of Rényi entropy  $S^{(2)}$  of the subsystem (1-10 qubits) by our neural network with the traditional quantum state tomography. It clearly shows that our machine learning approach is able to predict the entanglement information of the ground state of the 20-spin Hamiltonian without quantum state tomography. Meanwhile, in contrast to the  $4^{10} - 1$  (about one million) Pauli measurements that are required in 10-spin subsystem FST, our machine learning method only requires  $(20 - 1) \times 9 + 20 \times 3 = 231$  single-qubit and the nearest two-qubit Pauli measurements.

*Other models*-. More importantly, our machine learning approach can be easily extended to other Hamiltonians, including quantum  $l$ -local Hamiltonians, long-range interaction Hamiltonians, 2D Hamiltonian models, molecular systems relevant to quantum chemistry, etc. As a demonstration, we also test the application of our machine learning approach to estimating the entropy of the ground state of a long-range interaction Hamiltonian  $\mathcal{H}_{Long}$  and a 2D random Heisenberg model  $\mathcal{H}_{2D}$ .  $\mathcal{H}_{Long} = \sum_{i < j} J_0 / |i - j|^\alpha (X_i X_j + Y_i Y_j) + \sum B_i Z_i$  is the commonly considered model, such as the works [24, 29].  $\mathcal{H}_{2D} = \sum_{<ij>} J_{ij} (X_i X_j + Y_i Y_j + Z_i Z_j)$  is a 2D anti-ferromagnetic random Heisenberg model considered in the work [34]. Here, we consider only  $n = 6$  by exact diagonalization for the demonstration. The results are shown in Fig. 4(a). The demonstration on larger models can be obtained using DMRG (Density Matrix Renormalization Group).

*Comparison with existing methods*-. A detailed comparison with the existing method is presented here. First, our approach directly predicts the entropy of the subsystem without learning a prior on the classical representation of the quantum system. Current machine learning methods for quantum many-body systems typically learn a classical representation of the quantum system. However, since many measures of entanglement are not continuous, these may be insufficient for predicting entanglement. Namely, even if the learned state is very closely approximated by the actual state, the two may have significantly different values of entanglement. Our direct estimate of the entropy of the system avoids this problem. Second, our method directly measures

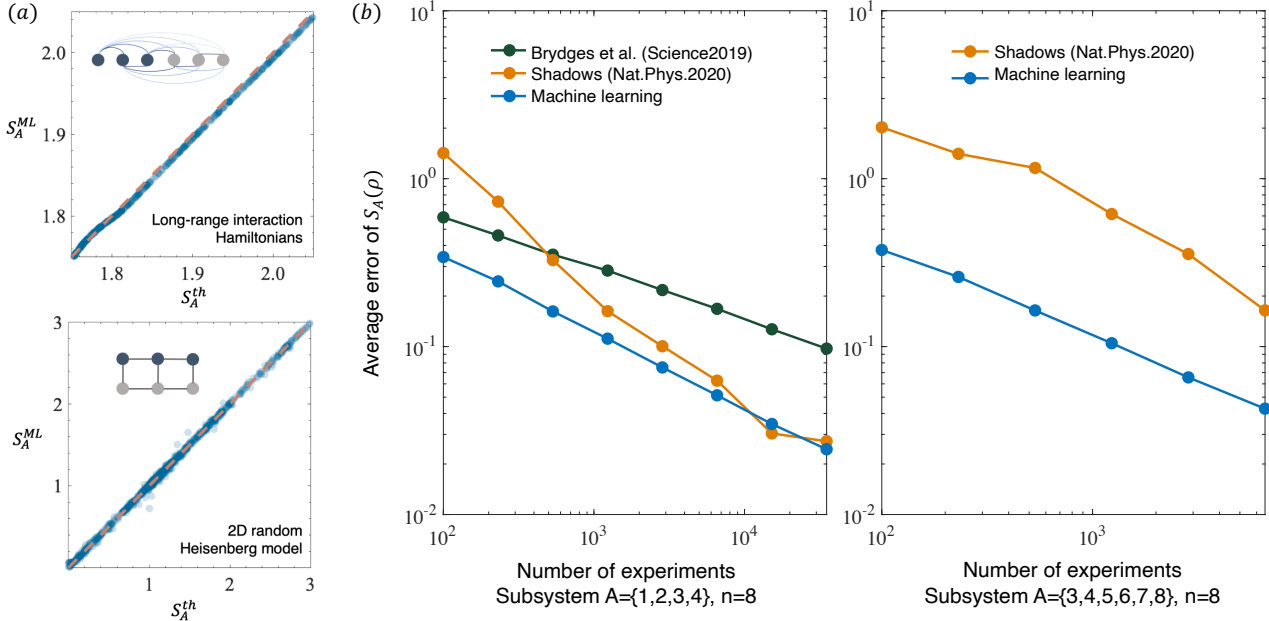


Figure 4. (a) The applications of our machine learning method in the model  $\mathcal{H}_{\text{Long}}$  and  $\mathcal{H}_{2D}$ . Here,  $S_A^{th}$  is the real entropy of the half-length subsystem and  $S_A^{ML}$  is the prediction result of our machine learning. (b) Comparison of our machine learning method with the randomized measurement toolbox proposed by T. Brydges *et. al.* [24] and the classical shadows proposed by Hsin-Yuan Huang *et. al.* [22] for predicting second-order entanglement entropy in 8-qubit ground states. Here, we consider the entanglement entropy of the subsystem  $A = \{1, 2, 3, 4\}$  and  $A = \{3, 4, 5, 6, 7, 8\}$ , respectively. It is well known that machine learning methods fail to achieve 100%-accurate predictions and their accuracy is limited by the machine learning model. Thus, machine learning methods lose their advantage when the number of experiments is infinite, but in practice a finite number of experiments are scheduled

129 the expectation value of the local Pauli operator, which is very easy to implement experimentally. There is a typical work that  
 130 directly predicts entanglement via machine learning [23], but it requires measurements of partially transposed moments as input,  
 131 which is very difficult to implement experimentally. To date, this work remains at the theoretical level for this reason.

132 In addition to machine learning methods, there are some well-known randomized methods for directly predicting the entropy  
 133 of a system, mainly including the randomized measurement toolbox and classical shadows [22, 24]. It is important to note  
 134 that these methods have their own strengths and weaknesses. Both the randomized measurement toolbox and the randomized  
 135 measurement toolbox work for any arbitrary states, but they require the exponential measurements in the subsystem size. Our  
 136 method is applicable for structured quantum states, such as the ground states and the dynamical states of quantum many-body  
 137 Hamiltonians (a molecular system relevant for quantum chemistry and  $l$ -local Hamiltonians), but it only requires polynomial  
 138 measurements. In this way, they form a complementary relation and are suitable for different applications in measuring the  
 139 second-order Rényi entropy of subsystems, where our approach would be a better choice for structured quantum states, as it  
 140 captures the central information and the classical shadows and random measurement toolbox would perform better for arbitrary  
 141 states. We have performed a comparison between our method, classical shadows, and the randomized measurement toolbox for  
 142 estimating the second-order Rényi entanglement entropy of subsystems in the ground states. Figure 4(b) shows the comparison  
 143 results. This clearly shows that our method requires fewer measurements and that the discrepancy will increase as we require  
 144 larger sizes.

### 145 Experimental demonstation

146 We also adopt our neural networks to predict static entanglement  $\mathcal{E}$  and non-equilibrium entanglement dynamics  $\mathcal{E}(t)$  on a  
 147 4-qubit nuclear magnetic resonance (NMR) platform [35, 36]. The used four-qubit sample is <sup>13</sup>C-labeled trans-crotonic acid  
 148 dissolved in *d*6-acetone, where four <sup>13</sup>C nuclear spins are encoded as a 4-qubit quantum processor. The internal Hamiltonian of  
 149 the system is given by

$$\mathcal{H}_{\text{int}} = - \sum_{i=1}^4 \pi \nu_i \sigma_z^i + \sum_{i,j}^4 \pi \frac{J_{ij}}{2} \sigma_z^i \sigma_z^j. \quad (2)$$

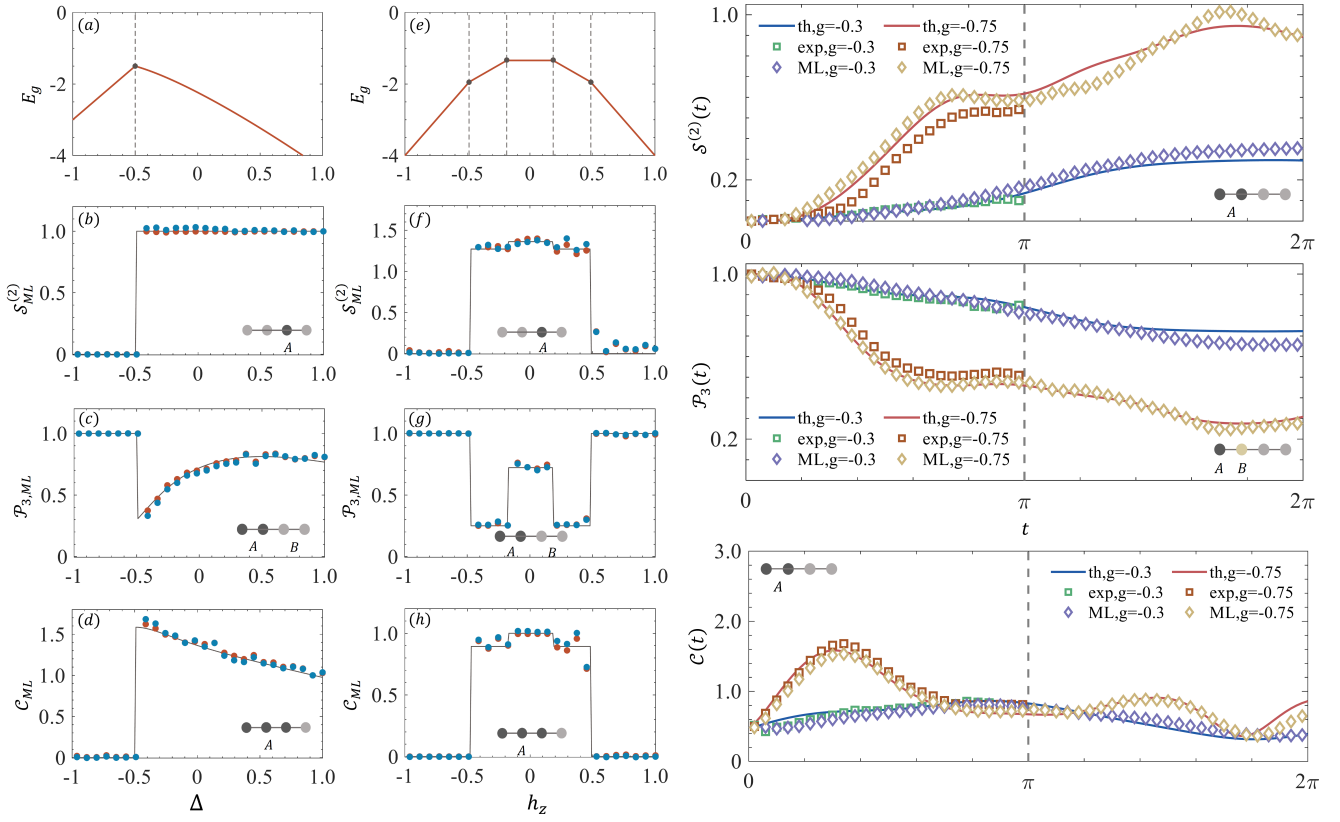


Figure 5. Left plot: Phase diagram of  $\mathcal{H}_{XXZ}$  and  $\mathcal{H}_{XX}$  models. (a) and (e) are the ground energy levels (red lines). (b-d) and (f-h) show the entanglement  $\mathcal{E}$  of the ground states of  $\mathcal{H}_{XXZ}$  and  $\mathcal{H}_{XX}$  models, respectively. Theoretical calculation (solid lines), quantum FST (red points), and our neural networks results (blue points) are distinguished. The measured subsystems are represented by the gray rounds schematic. Right plot: The dynamical evolution  $S^{(2)}(t)$  (the subsystem  $A = 12$ ),  $P_3(t)$  (the subsystems  $A = 1, B = 2$ ), and  $C(t)$  (the subsystem  $A = 12$ ) for two sets of parameters (i)  $J = -0.5, g = -0.3$  and (ii)  $J = -0.5, g = -0.75$ . The input layer only contains the measured single-qubit time traces in  $[0, \pi]$ . The trained model allows us to predict  $\mathcal{E}(t)$  in the training window  $[0, \pi]$  and in the unseen future time window  $[\pi, 2\pi]$ . The theoretical results (solid lines), quantum FST results (square dots), and predicted results (diamond dots), for the two setups, are each represented by a different color of identification line (or dot)

$\nu_i$  is the chemical shift of each spin, and  $J_{ij}$  is the coupling strength between different spins. The spin dynamics is controlled by shaped radio-frequency (rf) pulses [37]. The molecular structure and the Hamiltonian parameters can be found in the supplemental material[32]. All experiments were carried out on a Bruker 600-MHz spectrometer at room temperature.

First, we observe  $\mathcal{E}$  in two types of spin-half chains by studying the entanglement of their ground states. Their Hamiltonians are defined as  $\mathcal{H}_{XXZ} = -J \sum_{i=1}^3 (\sigma_x^i \sigma_x^{i+1} + \sigma_y^i \sigma_y^{i+1}) + \Delta \sum_{j=1}^3 \sigma_z^j \sigma_z^{j+1}$  and  $\mathcal{H}_{XX} = -J \sum_{i=1}^3 (\sigma_x^i \sigma_x^{i+1} + \sigma_y^i \sigma_y^{i+1}) + h_z \sum_{j=1}^4 \sigma_z^j$ . Their ground states exhibit jump across singularities characterized by sudden entanglement as a function of  $\Delta$  or  $h_z$  [38, 39].  $\Delta$  is the anisotropic parameter characterizing the magnetic field. In experiments, we prepare 50 ground states by changing  $\Delta$  and  $h_z$  from  $-1$  to  $1$  with a step of  $0.04$ , measure the expectation values of the two-local Pauli operators, and then use our trained neural network in Model 1 to predict the entanglement information of these states. Second, we investigate the non-equilibrium phenomena by characterizing the entanglement evolution  $\mathcal{E}(t)$  of the dynamical states of  $\mathcal{H}_d$ . Experimentally, we prepare the initial state  $|\psi_0\rangle = R_z(\pi/8)R_y(\pi/8)|0\rangle^{\otimes 4}$  and implement the dynamical evolution of the two Hamiltonians with the parameters  $J = -0.5, g = -0.3$  and  $J = -0.5, g = -0.75$ . We then measure the single-qubit time traces and use the trained neural network to predict the entanglement dynamics  $\mathcal{E}(t)$ . Here we also perform quantum FST on the ground states and dynamical states to provide a comparison with machine learning results.

Our experiment consists of the following steps. (i) *Initialization*. We first initialize the spins to pseudo-pure state (PPS)  $|0\rangle^{\otimes N}$  from the highly-mixed state via the selective-transition method [40–42]. Quantum FST was also performed to check the PPS quality. A fidelity of more than 99% provides a reliable initialization for the following experiments. (ii) *Preparing target states*. For the ground states of  $\mathcal{H}_{XX}$  and  $\mathcal{H}_{XXZ}$ , we optimize a 20 ms shaped pulse to drive the system to the target states from  $|0\rangle^{\otimes 4}$ . For the dynamical states of  $\mathcal{H}_d$ , we also optimize a 30 ms shaped pulse that realize the evolution  $\exp(-i\mathcal{H}_d t)$ . All shaped pulses are searched with the gradient ascent pulse engineering (GRAPE) technique [43]. (iii) *Measuring local information*. We measure the expectation values of  $\mathcal{O}$ . It consists of 39 Pauli measurements ( $3 \times 4$  single-qubit Pauli operators  $\{\sigma^i\}$ ,  $3 \times 9$  two-qubit Pauli

171 operators  $\{\sigma^i \sigma^{i+1}\}$ ) for the static models  $\mathcal{H}_{XXZ}$  and  $\mathcal{H}_{XX}$  [32]. For the dynamical states of  $\mathcal{H}_d$ , we measure 50 temporal points  
 172 from 0 to  $\pi$  with a step of  $\pi/50$  and measure  $3 \times 4$  single-qubit Pauli operators  $\{\sigma^i\}$  each moment. As an ensemble system,  
 173 NMR can easily measure the expectation value of the Pauli operators. (iv) *Predicting entanglement*. We first trained the neural  
 174 networks with 100,000 numerical training data for both the static and dynamic models. We then feed the measured data in the  
 175 above experiment step into the trained neural network to predict the entanglement of the target state.

176 The predictions of entanglement quantities by our neural networks display a singularity jump precisely where the theoretical  
 177 way occurs. In the left of Fig. 5, we show the static entanglement obtained by theoretical calculation (solid line), quantum FST  
 178 (red points), and our neural networks (blue points). In the  $\mathcal{H}_{XXZ}$  model, we set  $J = -0.5$ , and the singular point occurs when  
 179 the model reverts to an isotropic Heisenberg model ( $\Delta = J$ ). In the  $\mathcal{H}_{XX}$  model, we set  $J = -0.3$ , and we can observe the  
 180 magnetic critical point where the ground state energy levels cross ( $h_z = 2J \cos(\frac{k\pi}{5})$ , where  $1 \leq k \leq 4$  is an integer) [44]. In the  
 181 right of Fig. 5, we show the dynamical nature of the entanglement  $\mathcal{E}(t)$  in  $[0, 2\pi]$  using the measured single-qubit time traces.  
 182 Different dynamic behaviors will be observed in the cases of  $g < g_c$  and  $g > g_c$  [33]. When  $g = -0.3$ , the oscillation amplitude  
 183 of  $\mathcal{E}(t)$  (blue line) is modest and close to its initial value, and when  $g = -0.75$ ,  $\mathcal{E}(t)$  (red line) oscillates range is greatly larger  
 184 [32].

## 185 CONCLUSION

186 In summary, we have designed a machine learning-assisted strategy to estimate entanglement information from local measure-  
 187 ments for both ground and dynamical states. It can skip the challenging quantum FST, which in general requires an exponential  
 188 number of measurements. At the same time, for dynamical states, neural networks can keep track of long-term entanglement for  
 189 an unseen future time. We have furthermore verified the feasibility of our approach in practical 4-qubit NMR experiments.

190 A comparison with existing methods is presented here. Our approach directly measures the expectation value of the local Pauli  
 191 operator, which is very easy to implement experimentally, while typical work that directly predicts entanglement via machine  
 192 learning requires measurements of partially transposed moments as input, which is very difficult to implement [23]. Classical  
 193 shadows and the randomized measurement toolbox are two well-known methods for estimating entropy that work for arbitrary  
 194 states [22, 24], but they require exponential measurements in the subsystem size. Our approach is applicable to structured  
 195 quantum states, such as ground states and dynamical states of quantum many-body Hamiltonians, but requires only polynomial  
 196 measurements. In this way, they constitute complementary relations and are suitable for different applications in measuring  
 197 entropy. Our numerical experiments on the ground state clearly show that our method requires fewer measurements than them,  
 198 and the discrepancy increases as we require larger sizes [32].

199 Our neural network strategy has the following extensions and future applications. The previous research has demonstrated  
 200 that some quantum states can be determined using compressing sensing [45, 46], direct estimation [47], and the UD-property  
 201 (Uniquely Determined, UD) [17]. These techniques normally measure random or fixed Pauli measurements. This means that  
 202 by creating a nonlinear map with quantities like local expectation and entanglement, we can extend our framework to various  
 203 types of quantum states, such as UD-property quantum states [48]. In the future, we can test and improve the robustness  
 204 by incorporating noise into the training data. Third, our framework will have wide applications in studying the intriguing  
 205 equilibrium and non-equilibrium phenomena [49], because the entanglement entropy is an essential quantify that diagnoses and  
 206 characterizes QPTs [50], quantum thermalization [51], and quantum MBL [52].

207 **Data Availability.** The experimental data and the source code that support the findings of this study are available from the  
 208 corresponding author on reasonable request.

209 **Acknowledgments.** We thank Shi-Ju Ran and Peng-Fei Zhou for their help in generating training data via the tensor network.  
 210 This work is supported by the National Natural Science Foundation of China (12275117, 11905099, 12075110, 11975117,  
 211 11875159 and U1801661), Guangdong Basic and Applied Basic Research Foundation (2022B1515020074, 2019A1515011383,  
 212 2021B1515020070), National Key Research and Development Program of China (2019YFA0308100), Guangdong International  
 213 Collaboration Program (2020A0505100001), Science, Technology and Innovation Commission of Shenzhen Municipality  
 214 (ZDSYS20170303165926217, KQTD20190929173815000, JCYJ20200109140803865, JCYJ20170412152620376  
 215 and JCYJ20180302174036418), Shenzhen Science and Technology Program (Grants No. RCYX20200714114522109 and  
 216 No. KQTD20200820113010023), Pengcheng Scholars, Guangdong Innovative and Entrepreneurial Research Team Program  
 217 (2019ZT08C044), and Guangdong Provincial Key Laboratory (2019B121203002). Y. H. and L. C. contributed equally to this  
 218 work.

219 **Competing Interests.** The authors declare that there are no competing interests.

220 **Author Contributions.** T.X. conceived the idea of this paper. Y.H. and L.C. wrote and implemented the computer code and  
 221 simulations. C.W. accomplished the experiments. T.X., D.L., and J.L. supervised the project. Y.H., L.C., and C.W. wrote the

222 manuscript with feedback from all authors. Y.H., L.C., and C.W. contributed equally to this work.

---

- 223 [1] Horodecki, R., Horodecki, P., Horodecki, M. & Horodecki, K. Quantum entanglement. *Rev. Mod. Phys.* **81**, 865–942 (2009). URL <https://link.aps.org/doi/10.1103/RevModPhys.81.865>.
- 224 [2] Georgescu, I. M., Ashhab, S. & Nori, F. Quantum simulation. *Rev. Mod. Phys.* **86**, 153–185 (2014). URL <https://link.aps.org/doi/10.1103/RevModPhys.86.153>.
- 225 [3] Amico, L., Fazio, R., Osterloh, A. & Vedral, V. Entanglement in many-body systems. *Rev. Mod. Phys.* **80**, 517–576 (2008). URL <https://link.aps.org/doi/10.1103/RevModPhys.80.517>.
- 226 [4] Preskill, J. Quantum computing in the nisq era and beyond. *Quantum* **2**, 79 (2018). URL <https://quantum-journal.org/papers/q-2018-08-06-79/>.
- 227 [5] Gisin, N. & Thew, R. Quantum communication. *Nat. Photonics* **1**, 165–171 (2007). URL <http://www.nature.com/articles/nphoton.2007.22>.
- 228 [6] Lu, D. *et al.* Tomography is necessary for universal entanglement detection with single-copy observables. *Phys. Rev. Lett.* **116**, 230501 (2016). URL <https://link.aps.org/doi/10.1103/PhysRevLett.116.230501>.
- 229 [7] Sperling, J. & Vogel, W. Multipartite entanglement witnesses. *Phys. Rev. Lett.* **111**, 110503 (2013). URL <https://link.aps.org/doi/10.1103/PhysRevLett.111.110503>.
- 230 [8] Zwerger, M., Dür, W., Bancal, J.-D. & Sekatski, P. Device-independent detection of genuine multipartite entanglement for all pure states. *Phys. Rev. Lett.* **122**, 060502 (2019). URL <https://link.aps.org/doi/10.1103/PhysRevLett.122.060502>.
- 231 [9] Huber, M. & Sengupta, R. Witnessing genuine multipartite entanglement with positive maps. *Phys. Rev. Lett.* **113**, 100501 (2014). URL <https://link.aps.org/doi/10.1103/PhysRevLett.113.100501>.
- 232 [10] Frérot, I., Baccari, F. & Acín, A. Unveiling quantum entanglement in many-body systems from partial information. *PRX Quantum* **3**, 010342 (2022). URL <https://link.aps.org/doi/10.1103/PRXQuantum.3.010342>.
- 233 [11] Plenio, M. B. Logarithmic negativity: A full entanglement monotone that is not convex. *Phys. Rev. Lett.* **95**, 090503 (2005). URL <https://link.aps.org/doi/10.1103/PhysRevLett.95.090503>.
- 234 [12] Yu, X.-D., Imai, S. & Gühne, O. Optimal entanglement certification from moments of the partial transpose. *Phys. Rev. Lett.* **127**, 060504 (2021). URL <https://link.aps.org/doi/10.1103/PhysRevLett.127.060504>.
- 235 [13] Neven, A. *et al.* Symmetry-resolved entanglement detection using partial transpose moments. *npj Quantum Inf.* **7**, 152 (2021). URL <https://www.nature.com/articles/s41534-021-00487-y>.
- 236 [14] Cramer, M. *et al.* Efficient quantum state tomography. *Nat. Commun.* **1**, 149 (2010). URL <http://www.nature.com/articles/ncomms1147>.
- 237 [15] Torlai, G. *et al.* Neural-network quantum state tomography. *Nat. Phys.* **14**, 447–450 (2018). URL <http://www.nature.com/articles/s41567-018-0048-5>.
- 238 [16] Gross, D., Liu, Y.-K., Flammia, S. T., Becker, S. & Eisert, J. Quantum state tomography via compressed sensing. *Phys. Rev. Lett.* **105**, 150401 (2010). URL <https://link.aps.org/doi/10.1103/PhysRevLett.105.150401>.
- 239 [17] Xin, T. *et al.* Quantum state tomography via reduced density matrices. *Phys. Rev. Lett.* **118**, 020401 (2017). URL <https://link.aps.org/doi/10.1103/PhysRevLett.118.020401>.
- 240 [18] Xin, T. *et al.* Local-measurement-based quantum state tomography via neural networks. *npj Quantum Inf.* **5**, 109 (2019). URL <http://www.nature.com/articles/s41534-019-0222-3>.
- 241 [19] Xin, T. *et al.* Quantum pure state tomography via variational hybrid quantum-classical method. *Phys. Rev. Appl.* **13**, 024013 (2020). URL <https://link.aps.org/doi/10.1103/PhysRevApplied.13.024013>.
- 242 [20] Bengtsson, I. & Zyczkowski, K. *Geometry of Quantum States: An Introduction to Quantum Entanglement* (Cambridge University Press, 2006).
- 243 [21] Koutný, D. *et al.* *Deep learning of quantum entanglement from incomplete measurements* (Optica Publishing Group, 2022). URL <https://opg.optica.org/abstract.cfm?URI=QUANTUM-2022-QTh2A.4>.
- 244 [22] Huang, H.-Y., Kueng, R. & Preskill, J. Predicting many properties of a quantum system from very few measurements. *Nat. Phys.* **16**, 1050–1057 (2020). URL <http://www.nature.com/articles/s41567-020-0932-7>.
- 245 [23] Gray, J., Banchi, L., Bayat, A. & Bose, S. Machine-learning-assisted many-body entanglement measurement. *Phys. Rev. Lett.* **121**, 150503 (2018). URL <https://link.aps.org/doi/10.1103/PhysRevLett.121.150503>.
- 246 [24] Brydges, T. *et al.* Probing rényi entanglement entropy via randomized measurements. *Science* **364**, 260–263 (2019). URL <https://www.science.org/doi/10.1126/science.aaau4963>.
- 247 [25] Abanin, D. A., Altman, E., Bloch, I. & Serbyn, M. Colloquium: Many-body localization, thermalization, and entanglement. *Rev. Mod. Phys.* **91**, 021001 (2019). URL <https://link.aps.org/doi/10.1103/RevModPhys.91.021001>.
- 248 [26] Kaufman, A. M. *et al.* Quantum thermalization through entanglement in an isolated many-body system. *Science* **353**, 794–800 (2016). URL <https://www.science.org/doi/10.1126/science.aaf6725>.
- 249 [27] Altman, E. Many-body localization and quantum thermalization. *Nat. Phys.* **14**, 979–983 (2018). URL <http://www.nature.com/articles/s41567-018-0305-7>.
- 250 [28] Mazza, P. P. *et al.* Machine learning time-local generators of open quantum dynamics. *Phys. Rev. Research* **3**, 023084 (2021). URL <https://link.aps.org/doi/10.1103/PhysRevResearch.3.023084>.
- 251 [29] Elben, A. *et al.* Mixed-state entanglement from local randomized measurements. *Phys. Rev. Lett.* **125**, 200501 (2020). URL <https://journals.aps.org/prl/abstract/10.1103/PhysRevLett.125.200501>.

- [30] Baumgratz, T., Cramer, M. & Plenio, M. Quantifying coherence. *Phys. Rev. Lett.* **113**, 140401 (2014). URL <https://link.aps.org/doi/10.1103/PhysRevLett.113.140401>.
- [31] Xi, Z., Li, Y. & Fan, H. Quantum coherence and correlations in quantum system. *Sci. Rep.* **5**, 10922 (2015). URL <http://www.nature.com/articles/srep10922>.
- [32] See the supplemental material for details .
- [33] Nie, X. et al. Experimental observation of equilibrium and dynamical quantum phase transitions via out-of-time-ordered correlators. *Phys. Rev. Lett.* **124**, 250601 (2020). URL <https://link.aps.org/doi/10.1103/PhysRevLett.124.250601>.
- [34] Huang, H.-Y., Kueng, R., Torlai, G., Albert, V. V. & Preskill, J. Provably efficient machine learning for quantum many-body problems. *Science* **377**, eabk3333 (2022). URL <https://www.science.org/doi/abs/10.1126/science.abk3333>.
- [35] Jones, J. A. Quantum computing with nmr. *Prog. Nucl. Magn. Reson. Spectrosc.* **59**, 91–120 (2011). URL <https://linkinghub.elsevier.com/retrieve/pii/S0079656510001111>.
- [36] Gershenfeld, N. A. & Chuang, I. L. Bulk spin-resonance quantum computation. *Science* **275**, 350–356 (1997). URL <https://www.science.org/doi/10.1126/science.275.5298.350>.
- [37] Vandersypen, L. M. K. & Chuang, I. L. Nmr techniques for quantum control and computation. *Rev. Mod. Phys.* **76**, 1037–1069 (2005). URL <https://link.aps.org/doi/10.1103/RevModPhys.76.1037>.
- [38] Son, W., Amico, L., Plastina, F. & Vedral, V. Quantum instability and edge entanglement in the quasi-long-range order. *Phys. Rev. A* **79**, 022302 (2009). URL <https://link.aps.org/doi/10.1103/PhysRevA.79.022302>.
- [39] Zhang, J., Wei, T.-C. & Laflamme, R. Experimental quantum simulation of entanglement in many-body systems. *Phys. Rev. Lett.* **107**, 010501 (2011). URL <https://link.aps.org/doi/10.1103/PhysRevLett.107.010501>.
- [40] Cory, D. G., Fahmy, A. F. & Havel, T. F. Ensemble quantum computing by nmr spectroscopy. *Proc. Natl. Acad. Sci. U.S.A.* **94**, 1634–1639 (1997). URL <https://pnas.org/doi/full/10.1073/pnas.94.5.1634>.
- [41] Lu, D. et al. Simulation of chemical isomerization reaction dynamics on a nmr quantum simulator. *Phys. Rev. Lett.* **107**, 020501 (2011). URL <https://link.aps.org/doi/10.1103/PhysRevLett.107.020501>.
- [42] Lu, D., Brodutch, A., Li, J., Li, H. & Laflamme, R. Experimental realization of post-selected weak measurements on an NMR quantum processor. *New J. Phys.* **16**, 053015 (2014). URL <https://doi.org/10.1088/1367-2630/16/5/053015>.
- [43] Khaneja, N., Reiss, T., Kehlet, C., Schulte-Herbrüggen, T. & Glaser, S. J. Optimal control of coupled spin dynamics: design of nmr pulse sequences by gradient ascent algorithms. *J. Magn. Reson.* **172**, 296–305 (2005). URL <https://linkinghub.elsevier.com/retrieve/pii/S1090780704003696>.
- [44] Son, W., Amico, L., Plastina, F. & Vedral, V. Quantum instability and edge entanglement in the quasi-long-range order. *Phys. Rev. A* **79**, 022302 (2009). URL <https://link.aps.org/doi/10.1103/PhysRevA.79.022302>.
- [45] Donoho, D. Compressed sensing. *IEEE Trans. Inf. Theory* **52**, 1289–1306 (2006). URL <http://ieeexplore.ieee.org/document/1614066/>.
- [46] Flammia, S. T., Gross, D., Liu, Y.-K. & Eisert, J. Quantum tomography via compressed sensing: error bounds, sample complexity and efficient estimators. *New J. Phys.* **14**, 095022 (2012). URL <https://iopscience.iop.org/article/10.1088/1367-2630/14/9/095022>.
- [47] Flammia, S. T. & Liu, Y.-K. Direct fidelity estimation from few pauli measurements. *Phys. Rev. Lett.* **106**, 230501 (2011). URL <https://link.aps.org/doi/10.1103/PhysRevLett.106.230501>.
- [48] Roos, C. F. et al. Control and measurement of three-qubit entangled states. *science* **304**, 1478–1480 (2004). URL <https://www.Science.org/doi/abs/10.1126/science.1097522>.
- [49] Hinrichsen, H. Non-equilibrium critical phenomena and phase transitions into absorbing states. *Adv. Phys.* **49**, 815–958 (2000). URL <http://www.tandfonline.com/doi/abs/10.1080/00018730050198152>.
- [50] Peng, X., Du, J. & Suter, D. Quantum phase transition of ground-state entanglement in a heisenberg spin chain simulated in an nmr quantum computer. *Phys. Rev. A* **71**, 012307 (2005). URL <https://link.aps.org/doi/10.1103/PhysRevA.71.012307>.
- [51] Kaufman, A. M. et al. Quantum thermalization through entanglement in an isolated many-body system. *Science* **353**, 794–800 (2016). URL <https://www.science.org/doi/10.1126/science.aaf6725>.
- [52] Rispoli, M. et al. Quantum critical behaviour at the many-body localization transition. *Nature* **573**, 385–389 (2019). URL <http://www.nature.com/articles/s41586-019-1527-2>.